**Article type:** Article

**Title** Oxidation-Led Decomposition of Hexagonal Boron Nitride Coatings on Alloy Substrates at 900°C: Chromia-Formers

C. Fleming*

*Christopher Fleming*

Advanced Forming Research Centre, The Department of Design, Manufacture and Engineering Management, University of Strathclyde, 85 Inchinnan Drive, Inchinnan, Renfrewshire, PA4 9LJ, UK

christopher.fleming@strath.ac.uk

In contrast to a mass of powder in air at 900°C, the oxidation rate of hexagonal boron nitride does not tend to a plateau when present as a coating on austenitic stainless steel type 304 and type 310, and a real-world hot forming tool alloy. As with a mass of powder, a molten boron trioxide diffusion barrier encapsulates each hexagonal boron nitride grain around the basal plane. These subsequently merge to form a dispersion of remnant grains throughout a molten matrix. Boron trioxide is semipermeable, and as such, the substrate oxidises concurrently. As it does so, outwardly diffusing chromium (III) ions react with boron trioxide to form chromium borate, which depletes the diffusion barrier. This causes the oxidation of hexagonal boron nitride to be sustained at an enhanced rate and the overlayer ultimately undergoes complete decomposition. During this process, the scale comprises chromium borate and chromia only. Whilst manganese chromium spinel and iron chromium spinel form readily at the oxide-atmosphere interface of equivalently heat-treated uncoated substrates, they do not form until after the coating has completely decomposed.

Keywords: High Temperature Oxidation; Decomposition Reaction; Austenitic Steels; Ceramic Platelets; Metal forming

## 1 Introduction

It took over a century for hexagonal boron nitride (h-BN) to proceed from the initial synthesis stage in the early 1840s through to being a commercial material. In more recent years, however, as awareness of the unique combination of properties of this graphite analogue has proliferated, so too has its usage, in terms of both the scale and diversity of applications. As a gauge of this trend, the global market was valued at USD 658.11 million in 2017 and has been projected to reach USD 899.2 million by 2023. [1]

A significant share of this market is occupied by coatings that are used as high temperature lubricants and release agents within the metal forming sector. Typical applications include the hot forming and superplastic forming of titanium alloys at around 900°C, which are standard industrial methods for the manufacture of complex aerospace components. [2] These operations tend to be performed under an inert atmosphere; however, this is not always possible. In spite of this, there is an absence of published research into the fate of h-BN under oxidising conditions when present on substrates that are themselves susceptible to high temperature oxidation.

h-BN coatings are often applied to both the tool and the workpiece via the spraying, dipping or brushing of an evaporative suspension. [3] High temperature forming tools are typically manufactured from nickel-rich cast steels, with oxidation resistance enabled by high chromium content. Whilst the mechanical properties of these alloys may differ from those of compositionally similar 300 series austenitic stainless steels, the surface chemistry during

high temperature oxidation is qualitatively equivalent. [4] It was thus deemed valid, for reasons of practicality, to conduct the bulk of the investigations described herein on austenitic stainless steel type 304 (SS304) substrates. In order to assess the wider applicability of findings in terms of substrate susceptibility to oxidation, experiments were also conducted on austenitic stainless steel type 310 (SS310). This alloy comprises the same elements as SS304 but is significantly less susceptible to high temperature oxidation due to quantitative compositional differences.[5] Key experiments were then repeated on a real-world SPF tool alloy to establish the validity of drawing industrially relevant conclusions from this approach. The fate of h-BN coatings on the archetypal superplastic forming titanium alloy, Ti-6Al-4V, is described in a forthcoming complementary paper.

As with all alloys, when the chromia-formers of interest here are exposed to an oxidising atmosphere at high temperature, there is firstly an initial transient stage of oxidation. During this period, oxides form from all reactive alloy elements at the surface, in proportions approximately equivalent to their surface concentrations. [6] Thereafter, an adherent layer of chromia spreads laterally across the alloy-oxide interface. This layer is deemed protective as it retards both the inward diffusion of oxygen and the outward diffusion of alloy elements; nonetheless, it does not present an impermeable barrier. [7, 8] As such, with extended exposure, the oxide layers grow simultaneously at the alloy-oxide interface and the oxide-atmosphere interface. This results in scale that is composed of distinct layers.

After atmospheric exposure at 900°C for up to 50 hours, the scale on SS304 has been found to be bi-layered. The inner layer has been determined to be either solely chromia [9] or a solid solution of chromia and iron (III) oxide, [10] whilst the outer layer is either manganese chromium spinel [9] or a mixture of manganese chromium spinel and iron chromium spinel. [10] Indeed, after 24 hours at 900°C, the only ions that Wang et al. detected in the scale formed on a conventional polycrystalline SS304 were chromium (III), manganese (IV) and oxygen,

which suggests the presence of chromia and manganese chromium spinel only. [11] Given sufficient exposure, additional outer layers of iron-rich and nickel-rich oxides will grow.

The high temperature oxidation of h-BN powder has been well studied. Oxidation has been said to commence at 800°C [12-15] and it does so according to the three stoichiometric relationships in Equations 1(a)-(c). [13, 16]

$$BN(s) + \frac{3}{4}O_2(g) \rightarrow \frac{1}{2}B_2O_3(l) + \frac{1}{2}N_2(g) \qquad 1(a)$$

$$BN(s) + \frac{5}{4}O_2(g) \rightarrow \frac{1}{2}B_2O_3(l) + NO(g) \qquad 1(b)$$

$$BN(s) + \frac{7}{4}O_2(g) \rightarrow \frac{1}{2}B_2O_3(l) + NO_2(g) \qquad 1(c)$$

These equations have been calculated to have negative Gibbs free energies of reaction at 1 atm and 900°C; with $\Delta_{r(1(a))}G < \Delta_{r(1(b))}G < \Delta_{r(1(c))}G$. [16] Accordingly, nitrogen is the dominant gaseous product and the pressure of nitric oxide is approximately one order of magnitude greater than that of nitrogen dioxide. [17] Regardless of which reaction occurs, the only condensed phases in the system are h-BN and boron trioxide, and the mass increase for a given amount of reacted starting material is the same. With boron trioxide having a melting point in the region of 450°C, at 900°C it is molten and tacky with an absolute viscosity of 17.6 Pa $s^{-1}$. [18]

h-BN particles tend to possess a roundish, plate-like morphology [12, 15, 19, 20] and oxidation proceeds primarily around the basal plane peripheries, as opposed to the faces. [17, 20] As a powerful demonstration of the oxidation resistance of the h-BN basal plane, Liu et al. [21] found that a few large-scale layers of chemical vapour deposited h-BN could protect nickel and stainless steel foils at temperatures up to 1100°C in oxidising atmospheres. Similarly, graphene layer substrates could be protected up to 1000°C.

Whilst there has hitherto been no consensus in the literature as to which rate law best describes this system, it has been repeatedly shown that it commences rapidly and subsequently levels off. [12, 13, 16, 17, 20, 22] To explain this behaviour, Coles et al. proposed that as the h-BN particles become encompassed by molten boron oxide, they bind together. Thereafter, oxidation becomes increasingly controlled by liquid-state diffusion. [12] Similarly, Hou et al. propounded that as the boron oxide layer thickens, the powder particles connect together to form a compact bulk that impedes oxygen from reaching the reaction sites. [16, 22]

Boron trioxide is a hygroscopic material and, as such, in wet air it can react with atmospheric water vapour to form the volatile products metaboric acid ($HBO_2$) and orthoboric acid ($H_3BO_3$). Whilst Randall et al. [23] did not detect appreciable concentrations of metaboric acid when h-BN was oxidised below 1000°C in wet air, Cofer et al. detected metaboric acid and trace orthoboric acid at 700°C. [24] Hou et al. [16, 22] found an initial mass gain followed by linear mass loss at all temperatures investigated between 800°C and 1100°C in wet air. This was attributed to a steady state condition being established in which the oxidation and volatilisation rates were equal.

Whilst it was chosen to conduct this present investigation at 900°C because of the industrial relevance that has been described, the fate of the system at this temperature is particularly interesting because the coating and the substrate both oxidise at appreciable rates. Furthermore, all condensed phase oxidation products remain as such, i.e. at this temperature (i) the vaporisation of chromium (III) oxide via further oxidation into volatile chromium (VI) oxide [25] (ii) the volatility of boron trioxide [16, 26] and (iii) the loss of boron trioxide by reaction with ambient atmosphere water (as will be shown) are negligible.

## 2 Material and Methods

### 2.1 Materials

An evaporative, water based h-BN suspension incorporating a combustible organic binder system (HeBoCoat 20W) was obtained from *Henze Boron Nitride Products AG*. At the temperature of interest, the coating consisted purely of h-BN grains held together by weak cohesive forces, thereby enabling the interactions between h-BN, the substrate and oxygen only to be characterised. The h-BN powder in this formulation has a nominal particle size distribution of $D_{10}$=0.50 µm, $D_{50}$=4.90 µm, $D_{90}$=13.39 µm and $D_{100}$=27.00 µm, as stated by the manufacturer. Boron trioxide (Acros Organics, 99%) in granular form (40 mesh) was purchased from Fisher Scientific.

SS304 and SS310 coupons (50 x 50 x 5 mm) were purchased from West Yorkshire Steel Co Ltd and the supplier provided chemical compositions are detailed in Table 1. Tool material coupons were supplied by Rolls-Royce and the nominal composition is detailed in Table 1.

### 2.2 h-BN Coating Application and Heat-treatments

Coatings of reproducible thickness were applied to coupons using an automated spray system (Fanuc M-710iC industrial robot fitted with a Graco AirPro spray gun and linked to a Graco Pro Control 1KS Fluid Management System). Three thin coats were applied to each coupon and each coat was air dried for one hour before application of the next. The dry coating thicknesses were measured using an Elcometer 456.

Coated coupons, uncoated coupons and samples of the dried h-BN coating (in alumina-based ceramic crucibles) were heat-treated at 900°C in a Pyrotherm laboratory furnace, with the thermocouples calibrated to ASTM E220-13 using a Martel PTC8001 precision temperature calibrator. Exposure was followed by an air quench. In the case of the h-BN samples, the post heat-treatment product was removed carefully from the centre of the vessel to avoid material that may have reacted with the container, given that boron trioxide and alumina can react at 900°C to form aluminium borate. [16]

Oxidation rates of h-BN coated SS304 (10 x 10 x 5 mm) and the dry h-BN coating (15 mg) were assessed via thermogravimetric analysis (TGA), using Netszch STA 449 F1 Jupiter instrumentation. Temperature ramps up to 620°C were conducted in an 80% nitrogen: 20% oxygen mixture and thereafter continued to 900°C in nitrogen. The atmosphere was then switched back to the air mixture for the isothermal stage. This was to ensure that the binders had completely volatilised without h-BN oxidation having commenced when the reaction conditions were reached. In the case of the h-BN coated SS304 sample, it was not possible to apply the coating using the automated spray system so it was applied manually using a DeVilbiss Advance HD gravity feed spray gun. In lieu of being able to measure the thickness of the coating, the same procedure was followed and the coverage was deemed to have been complete and consistent by virtue of being uniformly white when dry.

**2.3 Surface Analysis**

Crystalline phase identification was achieved by x-ray diffraction (XRD) using a Bruker D8 Advance system with Cu Kα radiation, in conjunction with the International Centre for Diffraction Data (ICDD) PDF-2 2009 database. OriginPro 2015 was used to fit diffractogram peaks with a Gaussian-Lorentzian cross product function for the purposes of deconvolution and intensity calculations.

An FEI Quanta 250 field-emission gun scanning electron microscope (SEM) equipped with Oxford Instruments energy and wavelength dispersive spectroscopic electron probe microanalysis (EPMA) capabilities was used to observe surface morphologies and to determine the chemical compositions of near surface regions and absorbed entities. Due to h-BN and its oxide being electrically non-conductive, all samples were gold coated prior to analyses. Cross-sections were prepared by nickel plating the samples, followed by cold mounting and then cutting, grinding and polishing using non-aqueous lubricants.

## 3 Results

### 3.1 h-BN exposed to 900°C

#### *3.1.1 Dry Atmosphere*

The early rapid phase of oxidation followed by a slower phase that has been previously reported can be clearly seen in the Figure 1(a) TGA plot. [12, 13, 16, 17, 20, 22] The first derivative of this data reveals that there are actually three stages to the kinetics of oxidation of h-BN (Figure 1(b)). The rate of mass gain was initially, comparatively very fast and followed a linear rate law, which suggests that it was interface controlled. This is in contrast to the zero mass gain induction period that was reported by Shei et al. [15] The rate then dropped and continued to decrease gradually until a second, more pronounced attenuation occurred after approximately 12 hours, subsequent to which it almost plateaued.

Because of the simple mass balance in effect during the oxidation of h-BN in dry air at 900°C and the negligible volatility of boron trioxide at 900°C, [16, 26] it is a straightforward matter to determine the extent of reaction from TGA data. [16] If the reaction proceeded to completion, there would be a Δmass of +40.26%; thus, the measured 17.62% and 20.82% mass increases after 24 hours and 72 hours, respectively, indicate that 51.71% of the h-BN used in this study underwent oxidation after 72 hours at 900°C in dry air and only 7.95% (as a percentage of the starting material) was consumed between 24 and 72 hours.

#### *3.1.2 Ambient Laboratory Atmosphere*

The powder diffractograms from h-BN samples that were furnace heat-treated at 900°C for 24 hours and 72 hours are shown in Figure 2. The presence of h-BN and boron trioxide features only within the condensed phase of the heat-treated samples is consistent with the accepted reaction pathways detailed in stoichiometric equations 1(a)-(c). Boron trioxide is predominantly evident as the “hump”, which arises from the amorphous phase in which it is

almost always encountered. [27, 28] The marked levelling out of the oxidation rate in the TGA results can be appreciated here from the only slight decrease in the h-BN peak intensities and the commensurately slight increase in the boron trioxide hump with the additional 48 hours of exposure.

Given the tendency of boron trioxide to react with water and effectively vaporise in wet air at temperatures as low as 973 K, [24] it had to be determined whether this was a factor in the heat-treatment of h-BN at 900°C in the ambient laboratory atmosphere. These furnace-treated samples underwent a mass increase of 18.56% and 20.30% after 24 hours and 72 hours of exposure, respectively. The equivalency of these Δm values to those from the dry atmosphere TGA run indicates that it was not. By comparison, Hou et al. measured a net mass loss for exposures longer than 16 hours at 900°C in an atmosphere containing 6.5 wt.% water. [22]

### 3.2 SS304 exposed to ambient atmosphere at 900°C

SS304 coupons were furnace heat-treated at 900°C for various durations between 30 minutes and 64 hours. After 30 minutes, the surface had retained a metallic lustre and this had adopted a light brown colouration. The oxidised samples did not exhibit any sheen from 1 hour onwards, and the brown progressively darkened until it became an invariant black subsequent to 8 hours.

The evolution of oxide species can be followed in the diffractograms shown in Figure 3, which contain the strongest peaks of all reaction products. After 30 minutes, chromia and manganese chromium spinel had formed. SEM with EPMA revealed a complete coverage of small, densely packed grains of the former with sporadically located octahedral spinel crystallites atop. [4, 29] The broadening and shifting of the spinel (311) peak to a higher 2 theta value after 2 hours indicates that iron chromium spinel had also formed. This coincided with an apparently complete coverage of spinel being observed at the atmosphere interface.

Despite chromia no longer being discerned at this interface, the chromia peaks continued to increase in intensity with all further heat-treatments, which indicates chromia formation at the alloy-scale interface.

From 4 hours onwards, the (311) peak centre was essentially equidistant between that of manganese chromium spinel (35.24°) and iron chromium spinel (35.51°). Also post-4 hours, iron-rich chromium oxide was detected. Although the morphology of these latter crystallites was not readily definable, they formed distinctive clusters amongst the growing spinel. That the spinel and iron-rich chromium oxide peaks increased in intensity up to 64 hours without iron-rich chromium oxide forming a complete outer layer, indicates that the two species grew concurrently at the scale-atmosphere interface.

### 3.3 h-BN coated SS304 exposed to 900°C

#### *3.3.1 Thermogravimetric Analysis*

SS304 that was completely coated with an arbitrary thickness of h-BN was exposed to the same TGA program as the mass of h-BN powder (Section 3.1.1). The plots are shown alongside each other in Figure 1(a). With the mass of the substrate having been several orders of magnitude greater than that of the coating, the ordinate is expressed as a percentage of the initial mass of h-BN. It was not possible to separate the coating mass gain from that of the substrate.

As with isolated h-BN, the combined system underwent mass increases only, and these commenced at a short-lived, rapid and linear rate. This rate was greater with the substrate bound system.

The second stage of oxidation also occurred at a higher rate for the substrate bound h-BN. When the rate of $\Delta m$ started to level off, it did so after less time, after a greater proportional mass gain and with a more gradual curvature. Furthermore, rather than tending to a plateau,

the rate of mass gain increased at ca. 18 hours before steadily attenuating again during the latter stages of heat-treatment. At +109.24%, Δm after 72 hours of exposure was greater than the maximum possible Δm from the oxidation of h-BN. This is attributed to the coating and the substrate having oxidised concurrently.

The post-TGA sample was green in colour. Due to the small sample size, a 1.0 mm snout was used for XRD data collection at the post-TGA surface; consequently, the noise to signal ratio was high. This notwithstanding, it is clear that no h-BN or boron trioxide peaks and no amorphous hump were present in the resultant diffractogram (Figure 4). Further to the bulk substrate peak, chromium borate and chromia peaks were readily apparent, with the former the more pronounced of the two.

*3.3.2 Ambient atmosphere furnace tests*

*Characterisation of pre-heat treatment coatings*

The mean thickness of the dry coatings was 29.0 ± 2.8 µm. Atmosphere interface x-ray diffractograms showed peaks from h-BN and the alloy substrate only. The h-BN particles exhibited the typical planar structure, with smooth surfaces and curved edges. Subsequent to binder volatilisation, the coating comprised regions of haphazardly stacked, flatly oriented crystallites and agglomerations of variously oriented, smaller crystallites (Figure 5). The latter were possibly due to insufficient homogenisation prior to application. Whilst pores of the order of 1 µm were widespread, instances in which they penetrated the full thickness of the coating were negligible. The EPMA determined near surface composition was: 49.90±1.95 at.% boron, 47.09±2.49 at.% nitrogen, 2.78±1.68 at.% oxygen, < 1 at.% alloy elements (Table 2).

*Visual Developments*

The white, solid state h-BN coating became translucent and molten with extended exposure. This rendered the substrate observable, and it could be seen to have a distinct green colouration. As heat-treatment continued, the overlayer thinned until it could no longer be discerned. The substrate thereafter transitioned from green to black.

*Qualitative XRD Analysis*

The h-BN peaks progressively decreased in intensity throughout the heat treatments until 60 hours, at which point they had completely attenuated (Figure 6). Concurrently, boron trioxide features appeared and increased in intensity with exposure until 18 hours, after which they adopted an overall trend of attenuation. After 60 hours, they too had ceased to be detectable (Figure 6).

The loss of h-BN can be followed in an approximate sense from the areas of the Gaussian-Lorentzian cross product fits of the dominant (002) peak ($2\Theta$=26.74°) (Figure 7). Whilst the plotted data must be treated as qualitative because it does not take into account matrix effects or possible particle reorientation effects, it is clear that at no point during the heat-treatments did the rate of attenuation tend to a plateau. The (002) peak breadth was essentially invariant up to 3 hours of exposure, after which it underwent a pronounced narrowing. For all exposure times subsequent to 12 hours, the full width at half maximums were approximately 50% less than the initial values. This was possibly a consequence of a reduction of stacking faults or a relieving of microstrains over the course of the heat-treatments. As the decrease in h-BN particle size with oxidation can be expected to have led to peak broadening, the effects of the strain narrowing on this diffractogram feature must have been the most pronounced of these two competing factors.

XRD at the atmosphere interface subsequent to complete loss of h-BN and boron trioxide, revealed the presence of chromium borate, chromium oxide, manganese chromium spinel,

iron chromium spinel and iron-rich chromium oxide (Figure 8). The presence of parent alloy peaks in the diffractogram indicate that the analysis region covered the full thickness of the chemically reacted layer.

The fate of alloy elements within the interface region can be followed most clearly over the range 2θ=32-38°, which contains the most intense peaks from all the products of reactions involving these species (Figure 9). After 30 minutes of exposure, small amounts of chromia and spinel had formed. Thereafter, there was no further increase in spinel peak intensities until such time that h-BN and boron trioxide were no longer detected. After 1.5 hours, the chromia peaks had increased in intensity and a chromium borate (104) peak emerged as a shoulder on the high theta side of the chromia (104) peak. With subsequent exposure, the peaks from both species continued to increase in intensity, with chromium borate doing so at the greater rate. After 3 hours, the chromium borate (104) peak was the larger of the two, and this remained the case until 60 hours. After this exposure time, the chromia peak returned to being the more intense and significant amounts of manganese chromium spinel, iron chromium spinel and iron-rich chromium oxide were detected. It is not known whether the reduced chromium borate peak intensities in the longest exposure time diffractogram are a consequence of matrix effects or due to a loss of species.

*SEM and EPMA Analysis*

The reader is reminded that boron trioxide is molten at 900°C and that the microscale observations that follow describe each system subsequent to an air quench to room temperature. It is the hope that rapid surface cooling created sufficiently faithful snapshots of the system under reaction conditions to enable inferences to be made about the phenomena that occurred.

As oxidation commenced, the boundaries between individual grains became less distinct and the morphology of some of the grains can be seen to have changed from round to trigonal or hexagonal (Figure 10(a)). EPMA after 1.5 hours showed a reduced nitrogen content relative to boron. Significant oxygen and minor amounts of chromium, iron and manganese were also detected. These EPMA results, along with the others referred to in this section are contained within Table 2.

After 7.5 hours (Figure 10(b)), the uppermost entities had significantly increased in size and all possessed well-defined trigonal or, to a lesser extent, hexagonal planar morphologies. A considerable loss of granularity was apparent across the denser lower levels of the overlayer. In spite of this, these regions exhibited pronounced fine structure. The EPMA determined composition of the surface region showed a further significant nitrogen reduction and rise in oxygen, relative to boron. Chromium, iron and manganese remained at similar levels.

Commonplace across the surface after 12 hours of heat-treatment were stacked structures, with the uppermost entities being rounded and significantly smaller than those at lower structural levels (Figure 10(c)). An amorphous material devoid of fine structure can be discerned around the bases of some of the structures. Other than a further slight decrease in nitrogen and increase in oxygen, the EPMA results were comparable to those obtained from the 7.5 hours of exposure sample.

With further heat-treatment, the amorphous continuum became more widespread and morphologically well-defined entities were imaged in, what appears to be, a state of merging into it (Figure 10(d)). At 24 hours, the atmosphere interface comprised large plains interspersed by remnant structures (Figure 10(e)), which are likely a consequence of coating thickness inhomogeneities inherent to spray application. The plains were strewn with small

fissures (Figure 10(f)), and the boron, nitrogen and oxygen concentrations followed the preceding trends.

As oxidation of the systems continued, edge-like forms could be seen impressing upon the coating from below (Figure 10(g)) and as the coating proceeded to thin (as inferred from its increased transparency to the probe electrons), these sub-film species were rendered apparent as plate-like crystallites (Figure 10(h)). As previously, the EPMA interaction volume at these regions contained boron, nitrogen and oxygen, whilst chromium, manganese and iron were detected in sufficient quantities to be considered major components, with chromium being the most abundant.

In agreement with the XRD data, after 60 hours no coating remained on the substrates and in its place three classes of crystallite occupied the oxide-atmosphere interface (Figure 11(a)-(d)). Two of these exhibited either an octahedral or an undefinable morphology and were analogous to those observed on heat-treated uncoated SS304. Accordingly, EPMA showed these to be spinel and iron-rich chromium oxide, respectively (Table 3). The plate-like crystallites were not present on heat-treated uncoated SS304 and the composition of these was consistent with the chromium borate that was detected by XRD. No nitrogen was detected at the atmosphere interface of the post-coating samples.

The amorphous nature and diminished thickness of the oxidised coating can be appreciated from the cross section of the 48-hour heat-treated SS304 sample shown in Figure 12. To enable elemental analysis of solely the oxide layer after this exposure time, EPMA line scans were conducted over a region where the overlayer had not endured the sectioning process (Figure 13). The scale was approximately 5 µm thick and the transition from the alloy substrate can be seen to occur at 3 µm, where the iron and nickel counts dropped off sharply and the oxygen and manganese counts similarly increased. The chromium counts were fairly

consistent across the substrate selvedge and scale. No boron was present in the alloy and after a lag at the substrate side of the scale, the boron content increased towards the atmosphere interface. The nitrogen counts remained at the background noise level across the full length of the line scan, which is consistent with no nitrogen being detected at the atmosphere interface of the post-coating samples.

### 3.4 Boron trioxide coated SS304 exposed to ambient atmosphere at 900°C

SS304 coupons that were coated with ca. 100 µm thick films of boron trioxide were furnace heat-treated at 900°C for 30 minutes, 25 hours, 50 hours and 100 hours. Only boron trioxide and substrate peaks are present in the 30 minute diffractograms, despite the substrate having changed to a bright green colour; visible through the translucent coating. Thereafter, as with the h-BN coating experiments, chromia and chromium borate peaks emerged and grew (Figure 14). The presence of the former reveals that oxygen could diffuse through the molten overlayer to drive the oxidation of the alloy beneath, whilst the latter indicates that a reaction occurred between the boron trioxide and the substrate. Further to these reaction products, manganese borate ($MnB_4O_7$) peaks were also generated. No XRD evidence for the presence of manganese oxide species was found. SEM-based observations of the atmosphere interface of these heat-treated and quenched systems revealed a smooth and fissure-less film.

### 3.5 h-BN on other chromia-former alloys exposed to ambient atmosphere at 900°C

The phenomena that have been described were also observed when h-BN coated SS310 and h-BN coated real-world tool material were exposed to 900°C under ambient atmosphere. Crucially, the starting material and any boron trioxide that formed were completely consumed, and chromium borate was detected throughout the heat-treatments. No other borate species were detected. Where the substrate atmosphere interface was visible through

the overlayer, it exhibited a green colouration. Post-coating heating resulted in a proliferation of spinel and a colour change to black.

## 4 Discussion

The 900°C, ambient atmosphere fate of an h-BN coating on each of the three chromia-former alloy substrates that were investigated differed from that of a mass of h-BN powder. The generation of chromium borate in each system indicates that a reaction took place between the overlayer and the oxidising alloy, and it is propounded that this is the key to whether the oxidation rate tends to a plateau or continues to completion.

Initially, oxidation proceeded as has been reported for isolated h-BN powder. From the SEM-based analysis, it could be seen that from the shortest exposure times the boundaries between individual particles became less distinct and they tended to increase in size. This is consistent with the findings of Podobeda et al. who measured a decrease in specific surface area with oxidation. [14] It is similarly consistent with models that propose that a layer of molten boron trioxide forms around the individual basal plane peripheries, [17, 20] which causes them to agglomerate as it thickens. [12, 16, 22] This effect can be understood from the reaction stoichiometry and the molar volumes of h-BN and boron trioxide at 900°C, ca. 11.25 $cm^3$ $mol^{-1}$ and 45.18 $cm^3$ $mol^{-1}$, respectively. [18, 30]

To the best of the author's knowledge, the transition from being round plate-like to being distinctly trigonal or hexagonal plate-like has not previously been documented in h-BN oxidation studies. This could be due to the morphology of the agglomerates being more readily apparent when flat-lying as part of a coating rather than within a disordered mass. That the entities were so well defined supports the use of an air quench to adequately preserve each system in the reaction temperature state. It is suggested that the observed morphologies reflect the trigonal symmetry of the boron atoms comprising boron trioxide.

As oxidation continued, the uppermost layers of the stacked structures reduced in size and reverted to being rounded again. The comparable mass changes from the dry and ambient atmosphere heat-treatments of a mass of h-BN powder indicates that this was not due to boron trioxide reacting with atmospheric water to form volatile products. [16, 17, 24] Furthermore, the effects of such recession reactions would not be expected to become evident in the manner of a step change such as this. Rather, they would have been occurring at all prior stages of the heat-treatment where boron trioxide was present, yet the film entities hitherto progressively increased in size.

An alternative explanation is inferred from the continuous phases that interspersed the bases of the structures. This suggests that the molten boron trioxide had flowed from elevated positions towards the substrate, where it pooled; possibly after it had reached a critical mass. The effects of this pooling can be expected to be twofold: (i) a higher rate of h-BN oxidation could persist where the diffusion barrier was diminished (ii) the increased boron trioxide in the lower strata accelerated the merging of the partially oxidized structures into a continuum.

As the stacked structures merged across the surface, plains composed of boron, oxygen and low levels of nitrogen developed. The small fissures that were widespread across the surface are typical of a significant mismatch in coefficients of thermal expansion (CTE). As such, they may have formed upon cooling due to such a mismatch between (i) h-BN (which has a negative CTE in the direction of the basal plane up to 770°C [31]) and boron trioxide (which undergoes a liquid to solid phase transition at 450°C), and/or (ii) the overlayer and the substrate. That these fissures were not observed across the surface of the heat-treated boron trioxide on SS304, suggests that they were a consequence of the former of these possibilities.

From this evidence, it is reasoned that the plains were a dispersion of remnant h-BN throughout a boron trioxide dispersion medium, analogous to that which has been theorised

for a mass of oxidised h-BN powder. [22] From consideration of the TGA data, it is believed that this is akin to the third and final stage of oxidation of isolated h-BN, during which the continuous nature of a boron trioxide diffusion barrier causes the rate to tend to a plateau.

The oxidation rate of h-BN on chromia-former substrates, however, did not tend to a plateau and the starting material was ultimately completely consumed, along with the boron trioxide product.

One of properties of h-BN that has resulted in a proliferation of applications is its high degree of chemical inertness; [19] its oxide, however, is considerably less inert. [32-34] Thus, as boron trioxide and the substrate were found to react in the boron trioxide coated SS304 experiments, it is thought that this was also the reaction that led to the formation of chromium borate in the h-BN coated systems.

Given the high temperature oxidation mechanisms of chromia-former alloys, it is expected that there are two pathways by which this could have occurred (i) the formation of chromia, followed by reaction between chromia and boron trioxide, or (ii) reaction between outwardly diffusing chromium (III) ions and boron trioxide. It is believed that the latter of these occurred either predominantly or exclusively, for the following reasons:

1) The direct reaction between chromia and boron trioxide has been found to proceed to only a slight extent at 900°C. [35] In the systems under investigation here, the reactions that resulted in boron trioxide consumption and chromium borate formation proceeded to completion.
2) Whilst the formation of spinel was detected after the shortest heat-treatment, there was no evidence for the further formation of manganese or iron oxides until the h-BN and boron trioxide were entirely consumed; after which they formed readily. This was despite appreciable amounts of manganese and iron being detected at the scale-film interface.

This suggests that the presence of the continuous overlayer inhibited the formation of alloy element oxide species at this interface.

3) Whilst it is not known why manganese borate formed during the heat-treatment of boron trioxide coated SS304 but not the h-BN coated systems that were exposed to equivalent conditions, that no manganese oxide species were detected suggests that a reaction between oxide species did not occur. Similarly, in the analogous h-BN coated Ti-6Al-4V system, aluminium borate ($Al_4B_2O_9$) formed without aluminium oxide (to be described in a forthcoming paper).

Early in the heat-treatment, when the coating comprised discrete entities, outwardly diffusing chromium (III) ions encountered either boron trioxide or adsorbed oxygen; thus either chromium borate or chromia could form at the substrate outer-interface. Once the coating merged into a continuum, only chromium borate could form. This is reflected in the cross section analyses that showed a gradual increase in boron content across the thickness of the oxide layer. In support of this, is that where the overlayer was sufficiently transparent to SEM probe electrons, the only crystallites to be observed directly underneath were the platelets that were identified as chromium borate. Furthermore, the substrate was distinctly green, and this is colour of chromium borate. [35]

Stainless steel oxide layers grow simultaneously at the oxide-atmosphere interface and the alloy-oxide interface; hence, the boron-free region at the alloy-oxide interface was that which formed via inward oxygen diffusion. That this region was comparatively thin, indicates that the oxide layer grew predominantly via outward chromium cation diffusion. This is consistent with previous studies that have found that that chromium diffusion is more important than oxygen diffusion for chromia scale growth at 900°C. [36, 37]

The following explanation for what has been observed is thus put forth. At the early stages of heat-treatment, the h-BN basal planes became enveloped by boron trioxide, whilst oxygen

concurrently diffused through intergranular gaps in the coating to drive the oxidation of the substrate. Where boron trioxide formed in contact with the substrate, outwardly diffusing chromium (III) ions reacted with this material, with chromium borate as the product. Consumption of h-BN was initially greater than that of the oxide; hence, the volume around each grain periphery increased and merged, resulting in a dispersion of remnant h-BN through a molten boron trioxide matrix. This caused the short circuit diffusion paths to be cut off; however, oxygen was able to diffuse through this semi-permeable adlayer. As it did so, the substrate scale continued to grow. From this point, all outwardly diffusing chromium (III) ions reacted with the boron trioxide film. This depleted the protective diffusion barrier around the h-BN grains, with the consequence that oxidation continued at a higher rate than would be the case in the absence of a reactive substrate. This continued until the decomposition of both h-BN and its oxide were complete. This process is shown schematically in Figure 15. Thereafter, oxidation of the substrate proceeded as per the standard mechanisms and the atmosphere interface turned from green to black with a proliferation of alloy element ternary oxides.

On an applied level, this work has implications for titanium-alloy forming processes in both ambient and inert atmospheres. In the case of the former, and in accordance with the initial aims, the fate of h-BN tool coatings under process conditions has been elucidated. Further to this, however, the phenomena that have been observed may provide a ready means of cleaning up tools, irrespective of the process atmosphere. Over the course of a production run, coating tends to transfer from workpiece to tool upon contact. The transferred material accumulates and compacts with subsequent contact events and can be detrimental to part surface finish and geometry.[2, 38] As such, it is suggested that a period of 900°C exposure to ambient atmosphere may be sufficient to decompose adsorbed material and enable production runs to be prolonged.

On a fundamental level, the results that have been presented offer insight into an interesting system in which a metal and a ceramic undergo concurrent and interrelated high temperature corrosion.

## 5 Conclusions

1. When h-BN coated chromia-former alloys were exposed to ambient atmosphere at 900°C, molten boron trioxide formed around the individual h-BN basal plane peripheries. As the reacted layers thickened, the discrete entities merged into a dispersion of remnant h-BN throughout a boron trioxide matrix. Whilst this progression is equivalent to that which has been previously theorised for a mass of h-BN powder, this is the first time that it has been observed and documented on the microscale.
2. Unlike with similarly heat-treated h-BN powder, the emergence of a continuous boron trioxide diffusion barrier did not cause the rate of oxidation of an h-BN coating to tend to a plateau. This is because outwardly diffusing chromium (III) ions from the underlying substrate reacted with it to form chromium borate. Via this process, the protective layer existed in a depleted state.
3. With sufficient exposure, both h-BN and boron trioxide underwent complete decomposition. During this process, the alloy oxide layer comprised chromia and chromium borate only. With subsequent exposure, alloy element ternary oxides typical of the uncoated heat-treated substrates formed at the oxide-atmosphere interface.
4. This effect was observed on austenitic stainless steels type 304 and type 310, and on a real-world industrial hot forming tool alloy.

*Acknowledgements*

The author would like to thank Nicola Zuelli and Paul Blackwell for their invaluable support in enabling this study; Duncan Rodger and Jacqueline Schramm for their help when conducting the heat-treatment tests; Andy Pidcock and Tim Rose at Cranfield University for the nickel-plating and cross-sectioning of coupons for analysis; and Fiona Sillars and Tiziana Marrocco for their assistance at the Advanced Materials Research Laboratory, University of Strathclyde.

## 6 References

[1] Hexagonal Boron Nitride Market - Segmented by Type, Application, and Geography - Growth, Trends, and Forecast (2018–2023). Mordor Intelligence, yderabad, India, 2018. https://www.researchandmarkets.com/reports/4602286/hexagonal-boron-nitride-market-segmented-by

[2] P. A. Friedman, S. G. Luckey in High-temperature lubricants for superplastic forming of metals, Vol.  (Ed. G. Giuliano), Elsevier, Cambridge, 2011, pp.72-82.

[3] S. Rudolph Interceram. 1993, 42, 302-305.

[4] S. Baleix, G. Bernhart, P. Lours Mater. Sci. Eng., A. 2002, 327, 155-166.

[5] G. J. Yurek, D. Eisen, A. Garrattreed Metallurgical Transactions a-Physical Metallurgy and Materials Science. 1982, 13, 473-485.

[6] B. Chattopadhyay, G. C. Wood Oxidation of Metals. 1970, 2, 373-399.

[7] R. Lobnig, H. Schmidt, K. Hennesen, H. Grabke Oxidation of Metals. 1992, 37, 81-93.

[8] A. C. S. Sabioni, A. M. Huntz, J. Philibert, B. Lesage, C. Monty J Mater Sci. 1992, 27, 4782-4790.

[9] A. M. Huntz, A. Reckmann, C. Haut, C. Sévérac, M. Herbst, F. C. T. Resende, A. C. S. Sabioni Materials Science and Engineering: A. 2007, 447, 266-276.

[10] X. Peng, J. Yan, Y. Zhou, F. Wang Acta Materialia. 2005, 53, 5079-5088.

[11] S. Wang, M. Sun, H. Han, K. Long, Z. Zhang Corros Sci. 2013, 72, 64-72.

[12] N. G. Coles, D. R. Glasson, Jayaweer.Sa J Appl Chem. 1969, 19, 178-181.

[13] V. A. Lavrenko, A. F. Alexeev Ceram Int. 1986, 12, 25-31.

[14] L. Podobeda, A. Tsapuk, A. Buravov Powder Metallurgy and Metal Ceramics. 1976, 15, 696-698.

[15] M. D. Shieh, C. Lee Chem Eng Sci. 1993, 48, 1851-1857.

[16] X. M. Hou, Z. Y. Yu, Z. Y. Chen, K. C. Chou, B. J. Zhao J Am Ceram Soc. 2013, 96, 1877-1882.

[17] N. Jacobson, S. Farmer, A. Moore, H. Sayir J Am Ceram Soc. 1999, 82, 393-398.

[18] Napolitano.A, P. B. Macedo, E. G. Hawkins J Am Ceram Soc. 1965, 48, 613-616.

[19] A. Lipp, K. A. Schwetz, K. Hunold Journal of the European Ceramic Society. 1989, 5, 3-9.

[20] K. Oda, T. Yoshio J Mater Sci. 1993, 28, 6562-6566.

[21] Z. Liu, Y. J. Gong, W. Zhou, L. L. Ma, J. J. Yu, J. C. Idrobo, J. Jung, A. H. MacDonald, R. Vajtai, J. Lou, P. M. Ajayan Nat Commun. 2013, 4.

[22] H. Xinmei, L. Yanxiang, Y. Ziyou, C. Kuo-Chih International Journal of Applied Ceramic Technology. 2015, 12, E138–E145.

[23] S. P. Randall, J. L. Margrave Journal of Inorganic and Nuclear Chemistry. 1960, 16, 29-35.

[24] C. G. Cofer, J. Economy Carbon. 1995, 33, 389-395.

[25] E. A. Gulbransen, K. F. Andrew Journal of the Electrochemical Society. 1957, 104, 334-338.

[26] D. White, P. N. Walsh, H. W. Goldstein, D. F. Dever The Journal of Physical Chemistry. 1961, 65, 1404-1409.

[27] M. J. Aziz, E. Nygren, J. F. Hays, D. Turnbull J Appl Phys. 1985, 57, 2233-2242.

[28] G. E. Gurr, Montgome.Pw, C. D. Knutson, B. T. Gorres Acta Crystall B-Stru. 1970, B 26, 906-915.

[29] J. Akimoto, Y. Takahashi, Y. Gotoh, S. Mizuta Chemistry of Materials. 2000, 12, 3246-3248.

[30] V. L. Solozhenko, T. Peun Journal of Physics and Chemistry of Solids. 1997, 58, 1321-1323.

[31] R. S. Pease Acta Crystallogr. 1952, 5, 356-361.

[32] Y. Birol Mater Chem Phys. 2012, 136, 963-966.

[33] E. d. Frésart, S. S. Rhee, K. L. Wang Applied Physics Letters. 1986, 49, 847-849.

[34] J. D. Walton, N. E. Poulos J Am Ceram Soc. 1959, 42, 40-49.

[35] N. Tombs, W. Croft, H. Mattraw Inorganic Chemistry. 1963, 2, 872-873.

[36] R. Hussey, D. Mitchell, M. Graham Materials and Corrosion. 1987, 38, 575-583.

[37] S. C. Tsai, A. M. Huntz, C. Dolin Mater. Sci. Eng., A. 1996, 212, 6-13.

[38] P. E. Krajewski, A. T. Morales Journal of materials engineering and performance. 2004, 13, 700-709.

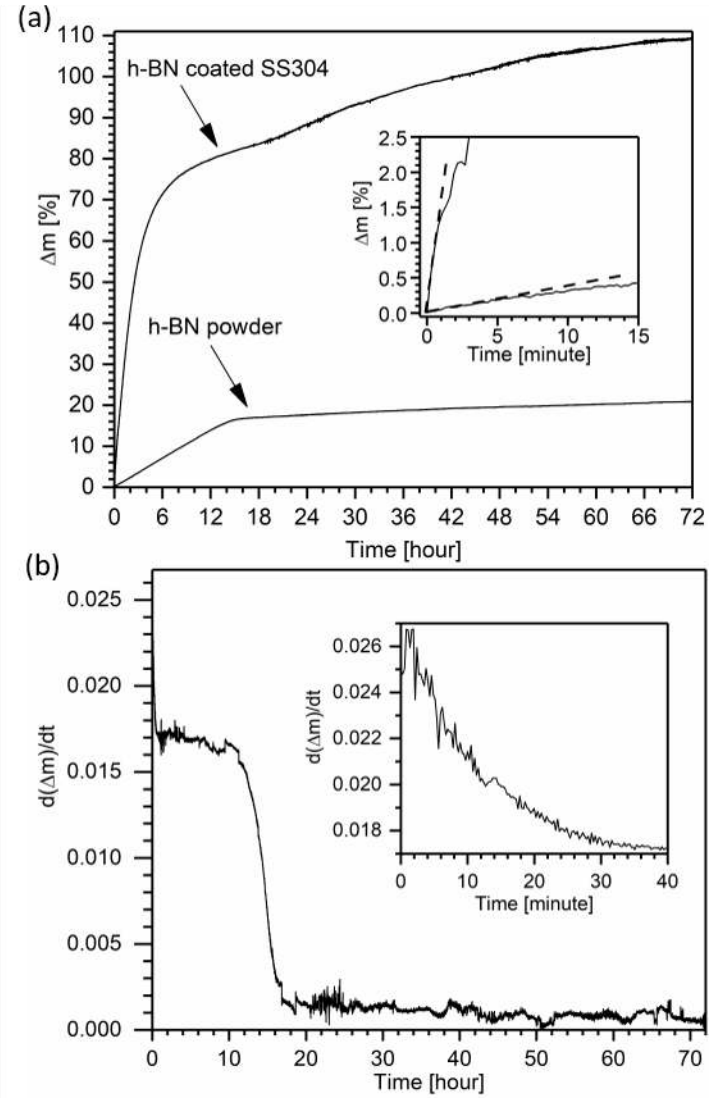


**Figure 1.** *(a) TGA plots from a mass of h-BN, and SS304 coated with an arbitrary thickness of h-BN that were exposed to a dry 80% $N_2$: 20% $O_2$ atmosphere for 72 hrs at 900°C. Inset is an expansion of the early stages of oxidation. The dashed lines are to highlight the initially linear rates of mass increase. (b) Derivative thermogravimetric curve from a mass of h-BN; inset is an expansion of the early stage of oxidation.*

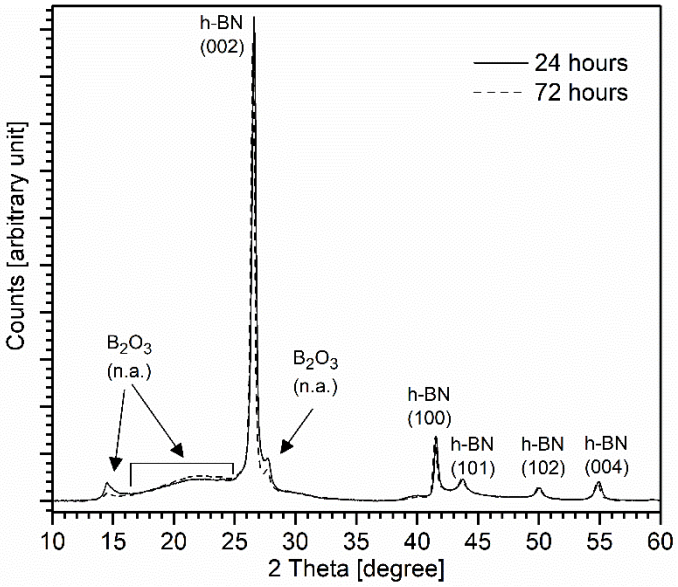


**Figure 2.** XRD plots from a mass of the h-BN coating that was heat-treated in ambient atmosphere at 900°C for 24 hours and 72 hours. The peaks are indexed according to the ICDD reference files: h-BN (PDF 00-034-0421) and $B_2O_3$ (PDF 00-013-0570).

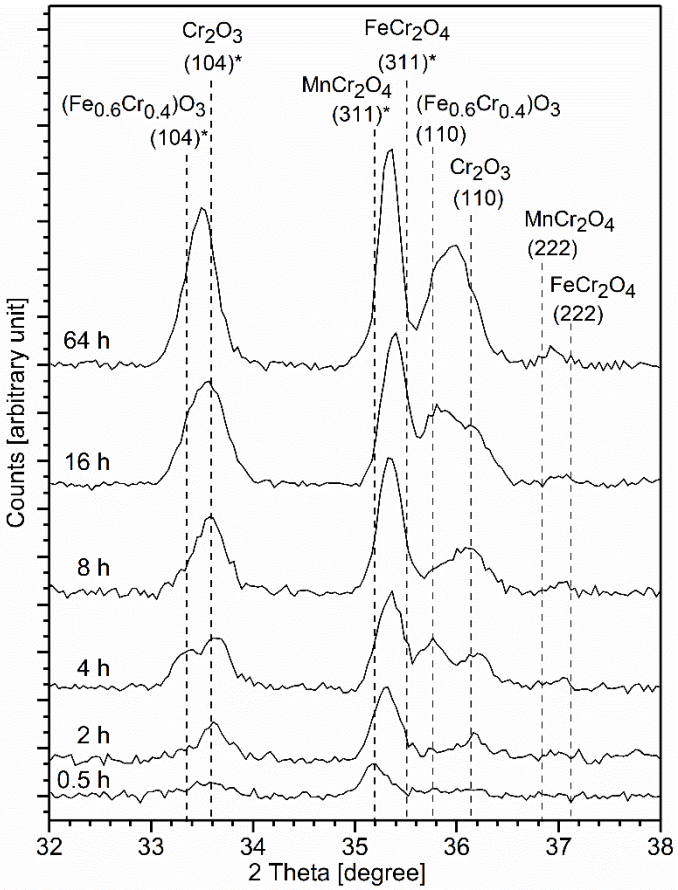


**Figure 3.** *XRD plots over the 2 Theta range 32°-38° from the atmosphere interface of uncoated SS304 that was heat-treated in ambient atmosphere at 900°C. The peaks are indexed according to the ICDD reference files: $Cr_2O_3$ (PDF 01-070-3765), $MnCr_2O_4$ (PDF 01-075-1614), $FeCr_2O_4$ (PDF 01-075-3312), $(Fe_{0.6}Cr_{0.4})O_3$ (PDF 00-034-0412). The strongest peak for each species is marked with an asterisk.*

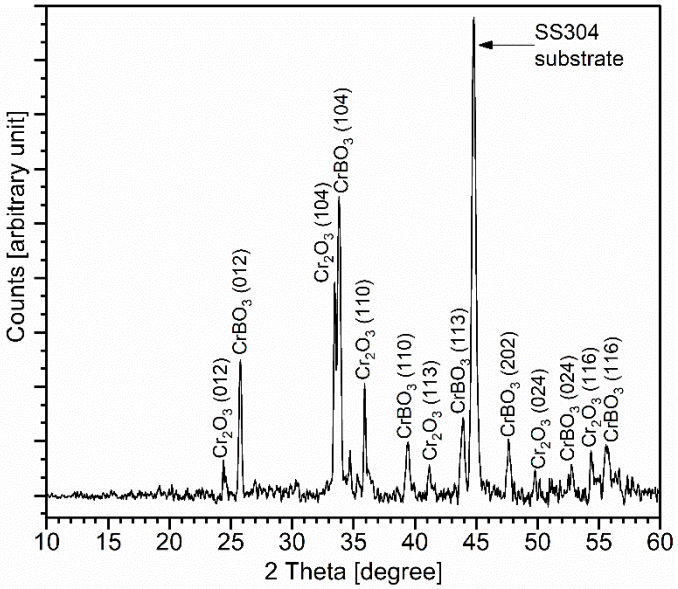


**Figure 4.** XRD plot from a face of the h-BN coated SS304 subsequent to having been exposed to dry air for 72 hrs at 900°C. The peaks are indexed according to the ICDD reference files: $CrBO_3$ (PDF 01-089-2658) and $Cr_2O_3$ (PDF 00-038-1479).

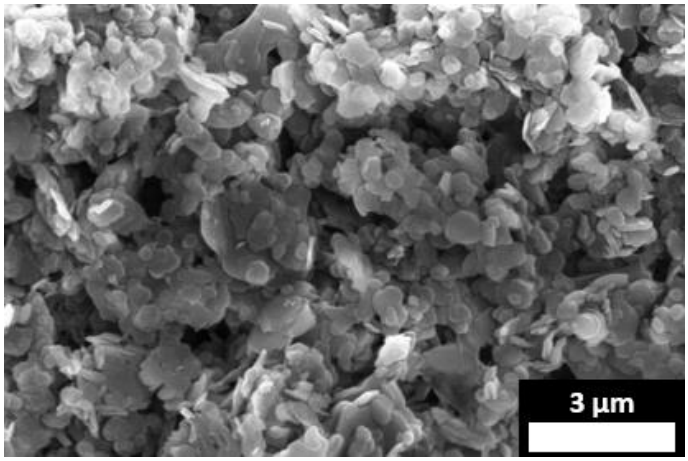


**Figure 5.** SEM micrograph showing the h-BN coating subsequent to volatilisation of organic binders.

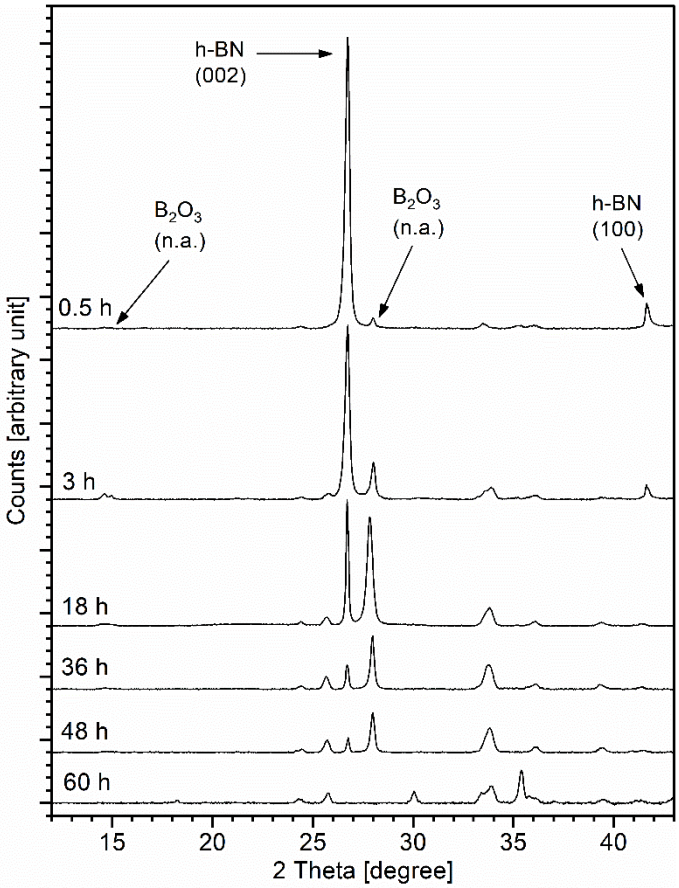


**Figure 6.** XRD plots at the atmosphere interface of h-BN coated SS304 that show the progression of h-BN (PDF 00-034-0421) and $B_2O_3$ (PDF 00-013-0570) peaks over the course of heat-treatment in ambient atmosphere at 900°C.

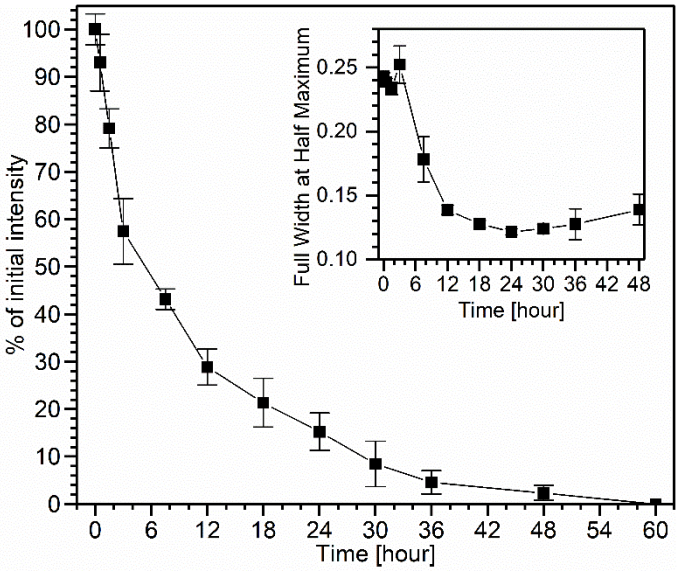


**Figure 7.** Intensity of the h-BN (002) peak after each heat-treatment duration at 900°C in ambient atmosphere, expressed as a percentage of that prior to heat-treatment. Inset is a plot of the full width at half maximum of this peak over the course of the heat-treatments. The error bars in each plot are the standard deviation of results from up to four individual samples.

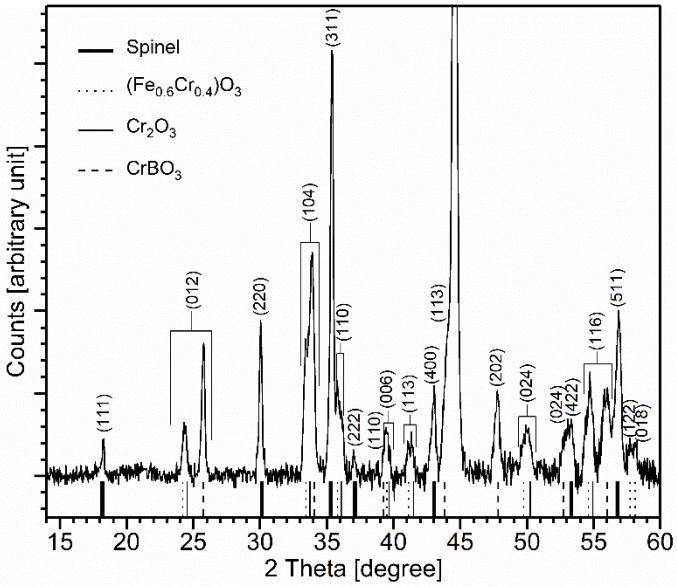


**Figure 8.** XRD plot at the atmosphere interface of h-BN coated SS304 after 60 hours of heat-treatment in ambient atmosphere at 900°C. The peaks are indexed according to the ICDD reference files: spinel ($MnCr_2O_4$ (PDF 01-075-1614)/$FeCr_2O_4$ (PDF 01-075-3312)), $Cr_2O_3$ (PDF 01-070-3765), $CrBO_3$ (PDF 01-089-2658) and $(Fe_{0.6}Cr_{0.4})O_3$ (PDF 00-034-0412). The dominant alloy peak at $2\theta = 44.59°$ has been truncated to aid clarity.

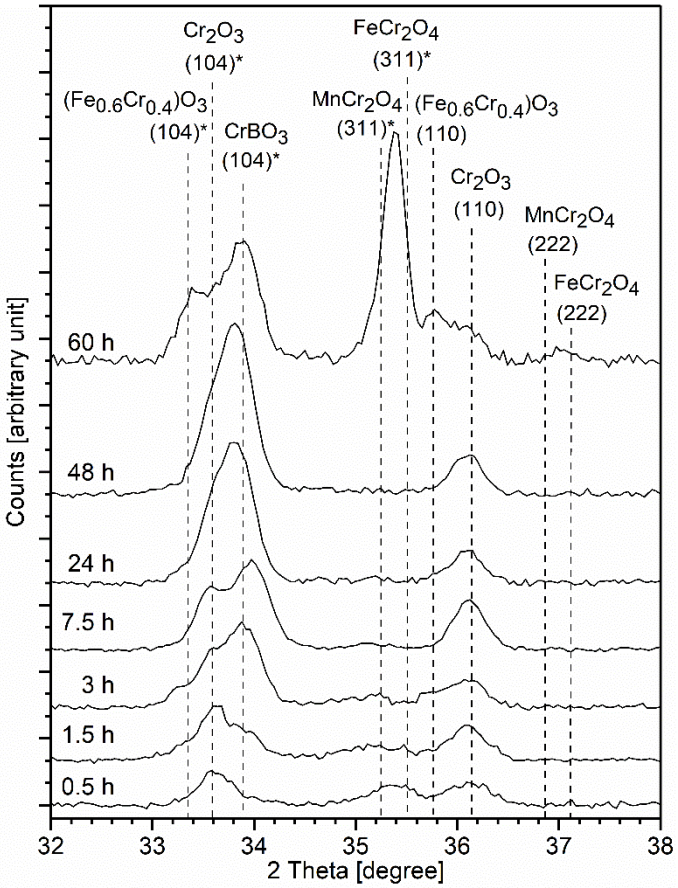


**Figure 9.** XRD plots over the 2 Theta range 32°-38° from the atmosphere interface of h-BN coated SS304 that was heat-treated in ambient atmosphere at 900°C. The peaks are indexed according to the ICDD reference files: $Cr_2O_3$ (PDF 01-070-3765), $MnCr_2O_4$ (PDF 01-075-1614), $FeCr_2O_4$ (PDF 01-075-3312), $(Fe_{0.6}Cr_{0.4})O_3$ (PDF 00-034-0412) and $CrBO_3$ (PDF 01-089-2658). The strongest peak for each species is marked with an asterisk.

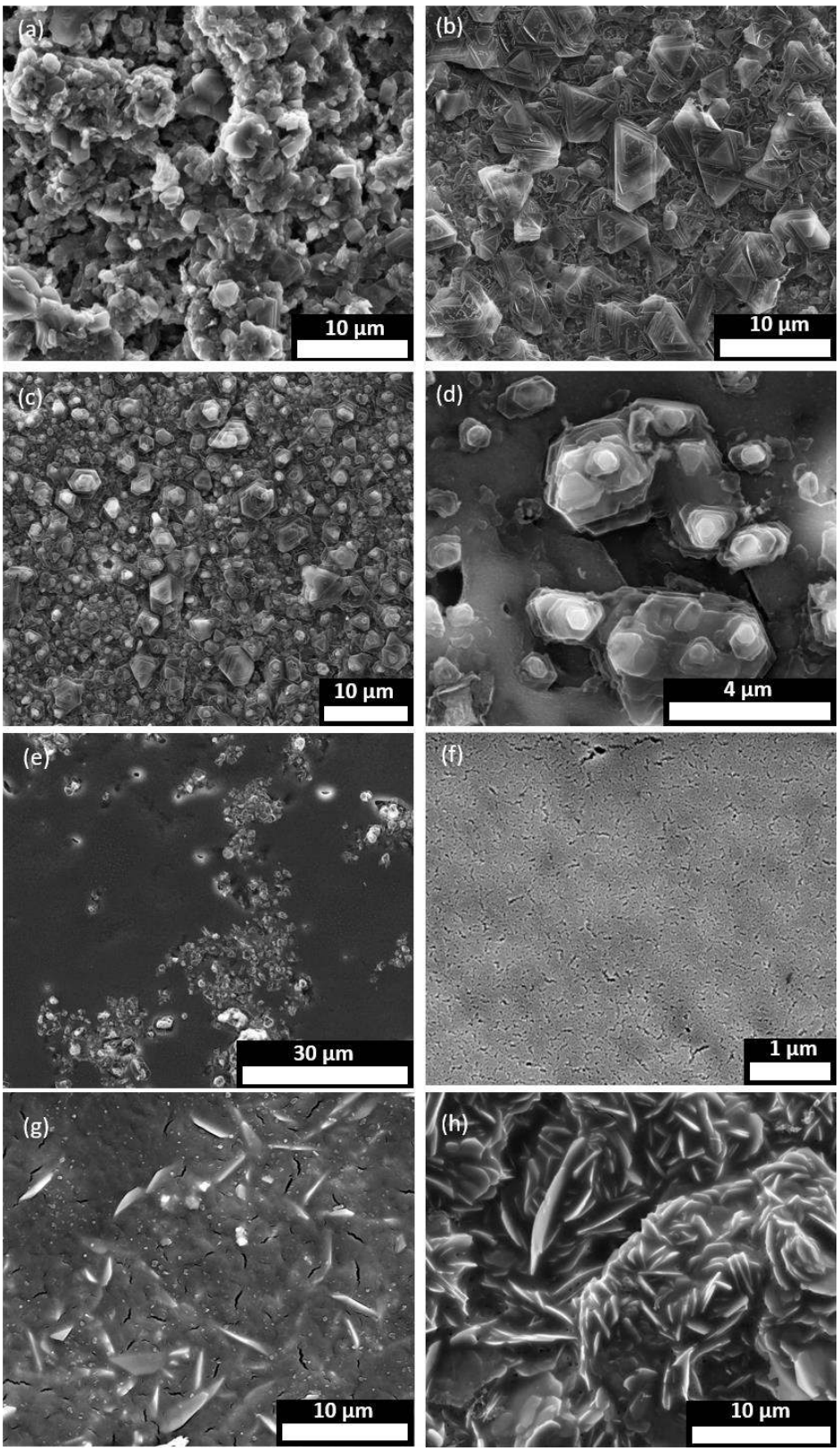


**Figure 10.** SEM micrographs showing the developments at the h-BN coated SS304 atmosphere interface during heat-treatment in ambient atmosphere at 900°C for: (a) 1.5 h (b) 7.5 h (c) 12 h (d) 18 h (e) 24 h (f) 24 h, (g) 36 h (h) 48 h.

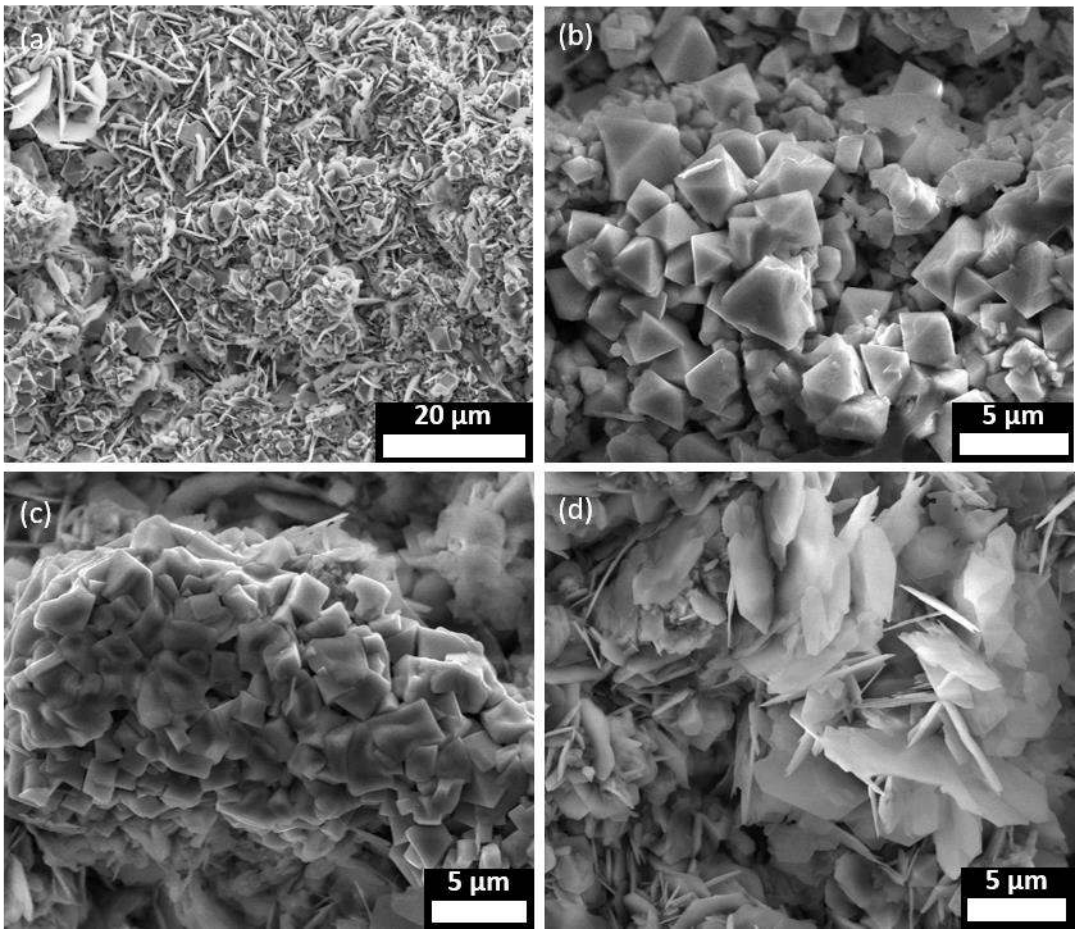


**Figure 11.** *SEM micrographs detailing the species present at the atmosphere interface of h-BN coated SS304 subsequent to 60 hours of heat-treatment in ambient atmosphere at 900°C. (a) Typical surface region (b) spinel (c) chromium borate (d) iron-rich chromium oxide.*

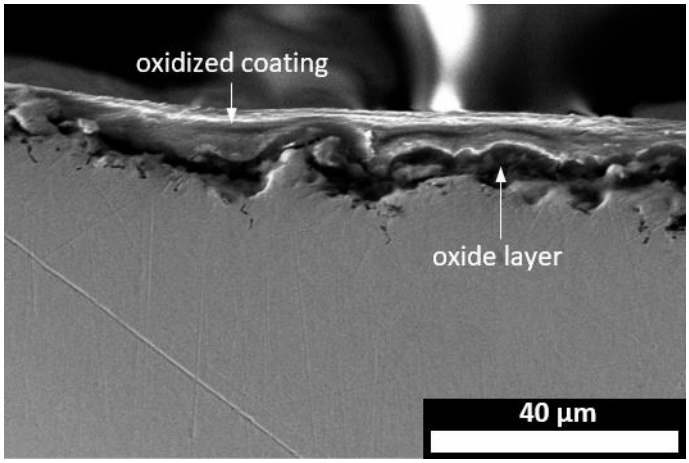


**Figure 12.** SEM micrograph showing the upper region of the cross section of h-BN coated SS304 that was heat-treated for 48 hours at 900°C in ambient atmosphere. The oxidised film, scale and substrate are observable.

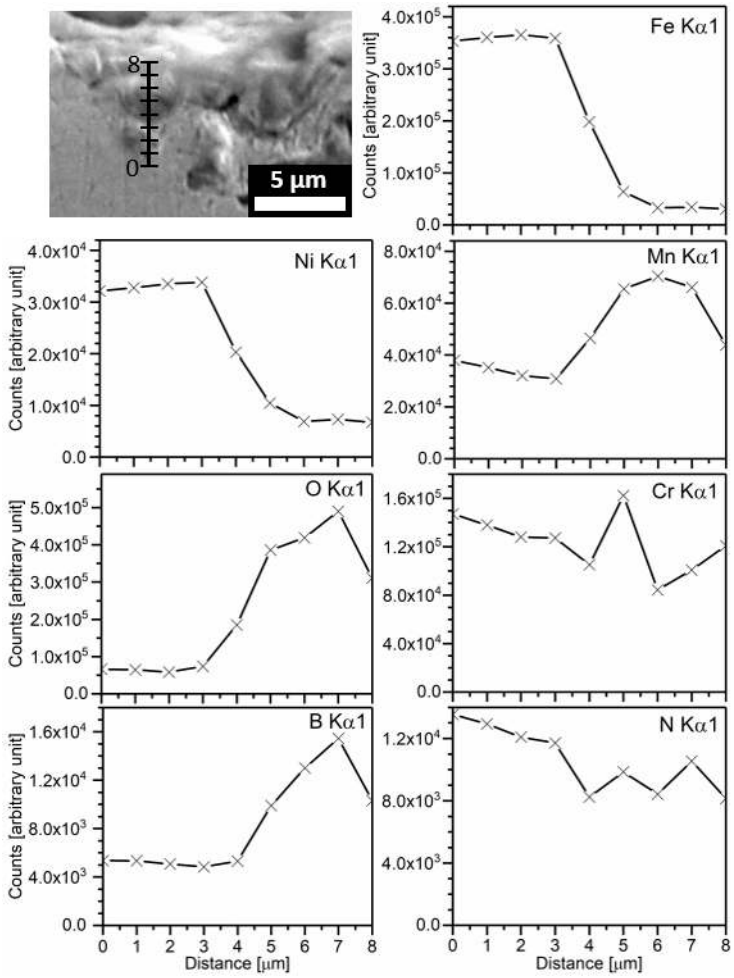


**Figure 13.** EPMA line scans that qualitatively detail the elemental composition through the depth of the oxide layer that formed on h-BN coated SS304 exposed to 900°C for 48 hours in ambient atmosphere. Top left is an SEM micrograph showing the cross section region that was analysed.

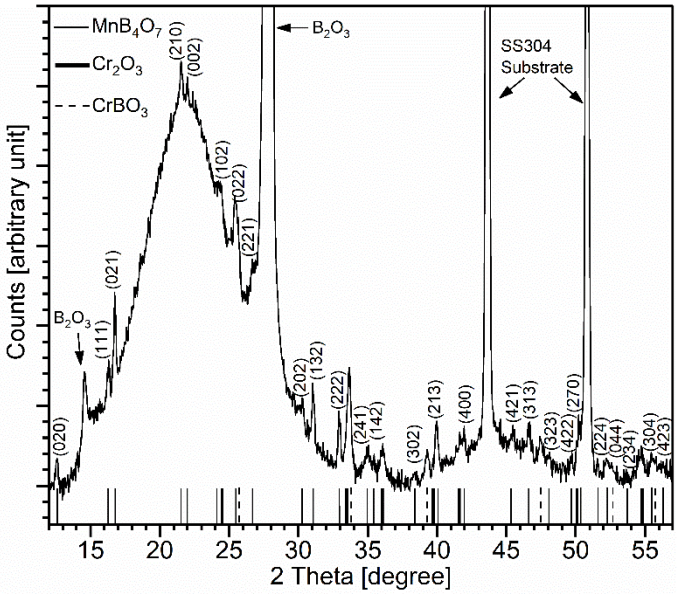


**Figure 14.** *XRD plot at the atmosphere interface of $B_2O_3$ coated SS304 after 100 hours of heat-treatment in ambient atmosphere at 900°C. The peaks are labelled according to the ICDD reference files: $MnB_4O_7$ (PDF 01-070-2045), $Cr_2O_3$ (PDF 01-070-3765), $CrBO_3$ (PDF 01-089-2658) and $B_2O_3$ (PDF 00-013-0570). For clarity, the ordinate is shown over a reduced range and only the $MnB_4O_7$ peaks are indexed; $Cr_2O_3$ and $CrBO_3$ peaks are as previously.*

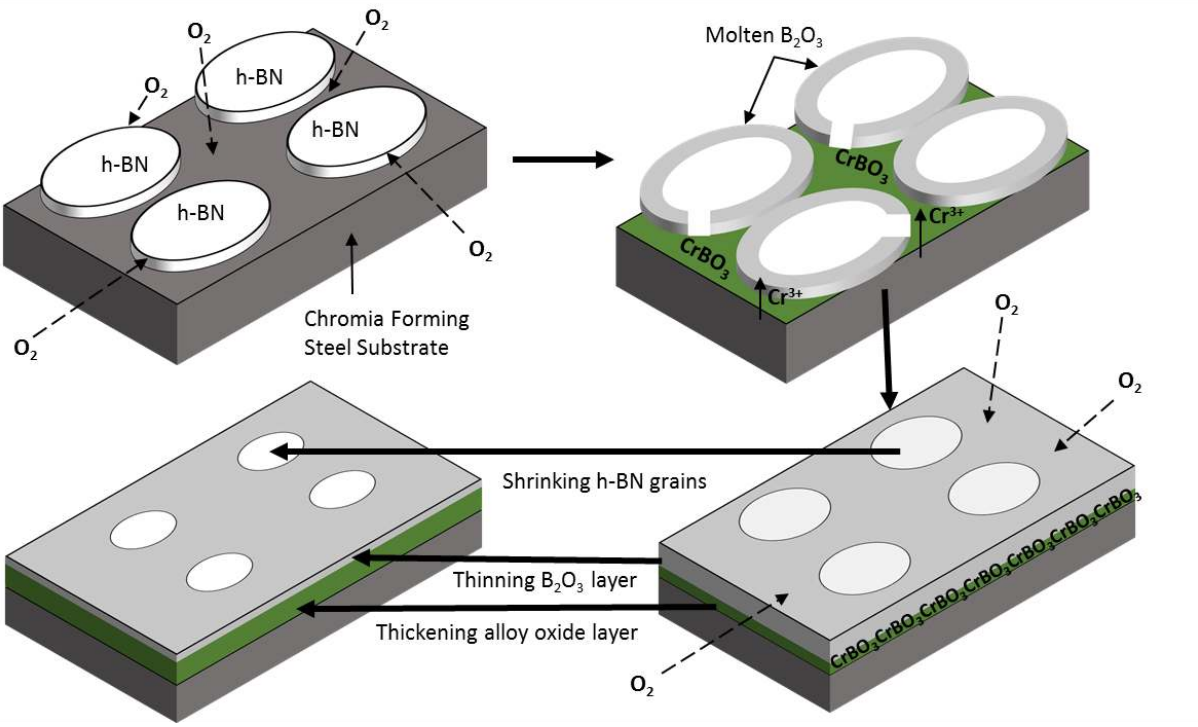


**Figure 15.** Schematic of the proposed reaction mechanisms that lead to complete decomposition of an h-BN coating on chromia-former alloy substrates in ambient atmosphere at 900°C. To aid clarity, only a single layer of h-BN is shown and the intergranular gaps have been exaggerated.

**Table 1.** wt.% compositions of the chromia-former alloy substrates used.

| | Fe | Cr | Ni | Mn | C | Si | S | P |
|---|---|---|---|---|---|---|---|---|
| SS304 | Bal | 18.1 | 8.0 | 1.87 | 0.021 | 0.48 | 0.001 | 0.032 |
| SS310 | Bal | 24.3 | 19.2 | 1.77 | 0.043 | 0.45 | 0.002 | 0.021 |
| SPF Tool | 27 | 18 | 52 | 1 | 0.5 | 1.5 | - | - |

**Table 2.** EPMA determined compositions at the atmosphere interface of the heat-treated h-BN coated SS304 systems after various exposure times at 900°C. Each result is the mean of ten analysis regions akin to those shown in the corresponding SEM micrographs. All compositions are given in at.%.

| | B | N | O | Cr | Fe | Mn | Ni |
|---|---|---|---|---|---|---|---|
| No heat-treatment (Figure 5) | 49.9 ± 2.0 | 47.1 ± 2.5 | 2.8 ± 1.7 | <1 | <1 | 0 | 0 |
| 1.5 hours (Figure 10(a)) | 37.0 ± 2.1 | 20.0 ± 1.8 | 42.5 ± 3.7 | <1 | <1 | <1 | 0 |
| 7.5 hours (Figure 10(b)) | 30.2 ± 2.7 | 4.5 ± 0.5 | 64.9 ± 3.1 | <1 | <1 | <1 | 0 |
| 12 hours (Figure 10(c)) | 29.5 ± 1.8 | 2.6 ± 0.5 | 67.6 ± 2.0 | <1 | <1 | <1 | 0 |
| 24 hours (Figure 10(f)) | 23.9 ± 2.2 | 2.2 ± 0.2 | 73.4 ± 1.5 | <1 | <1 | <1 | 0 |
| 48 hours (Figure 10(h)) | 23.8 ± 3.2 | 1.4 ± 0.3 | 63.3 ± 1.2 | 8.1 ± 2.4 | 2.2 ± 0.6 | 1.3 ± 0.7 | <1 |

**Table 3.** EPMA results from the analysis windows comprising the micrographs in Figure 11(b)-(d), which show the three types of crystallite present at the atmosphere interface of the 60-hour h-BN on SS304. All compositions are given in at.%.

| | B | N | O | Cr | Fe | Mn | Ni |
|---|---|---|---|---|---|---|---|
| Figure 11(b): spinel $(Mn,Fe)Cr_2O_4$ | 0 | 0 | 56.4 | 24.1 | 5.3 | 13.3 | 0.9 |
| Figure 11(c): iron-rich chromium oxide $(Fe_{0.6}Cr_{0.4})O_3$ | 0 | 0 | 58.8 | 14.5 | 22.7 | 3.4 | 0.6 |
| Figure 11(d): chromium borate $CrBO_3$ | 14.1 | 0 | 65.3 | 17.1 | 1.2 | 2.2 | 0.1 |

**Graphical Abstract**

Hexagonal boron nitride is widely used in industry as a high temperature tool coating. The fate of this material on representative chromia-former alloy substrates was investigated in air at 900°C. As the coating and substrate oxidised concurrently, chromium (III) ions reacted with boron trioxide to generate chromium borate. This ultimately resulted in complete decomposition of the coating.

ToC figure